A Study on Wildfire Impacts on Greenhouse Gas Emissions and Regional Air Quality in South of Orléans, France

Chaoyang Xue[1], Gisèle Krysztofiak[1], Yangang Ren[2, 3], Min Cai[2], Patrick Mercier[4], Frédéric Le Fur[4], Corinne Robin[4], Benoit Grosselin[2], Véronique Daële[2], Max R. McGillen[2], Yujing Mu[3], Valéry Catoire[1, *], Abdelwahid Mellouki[2, 5, *]

[1] Laboratoire de Physique et Chimie de l'Environnement et de l'Espace (LPC2E), CNRS – Université Orléans – CNES (UMR 7328), 45071 Orléans Cedex 2, France

[2] Institut de Combustion, Aérothermique, Réactivité Environnement (ICARE), CNRS, 45071 Orléans Cedex 2, France

[3] Research Centre for Eco-Environmental Sciences, Chinese Academy of Sciences, Beijing 100085, China

[4] Lig'Air- Association de surveillance de la qualité de l'air en région Centre-Val de Loire, 45590 Saint-Cyr-en-Val, France

[5] Mohammed V University, Rabat, Morocco

Correspondence:

Abdelwahid Mellouki (mellouki@cnrs-orleans.fr)

Valéry Catoire (valery.catoire@cnrs-orleans.fr)

Abstract

Wildfire events are increasing globally which may be partly associated with climate change, resulting in significant adverse impacts on local, regional air quality and global climate. In September 2020, a small wildfire (burned area: 36.3 ha) event occurred in Souesmes (Loir-et-Cher, Sologne, France), and its plume spread out over 200 km on the following day as observed by the MODIS satellite. Based on measurements at a suburban site (~50 km northwest of the fire location) in Orléans and backward trajectory analysis, young wildfire plumes were characterized. Significant increases in gaseous pollutants (CO, CH_4, N_2O, VOCs, etc.) and particles were found within the wildfire plumes, leading to a reduced air quality. Emission factors of various trace gases and black carbon were determined accordingly and compared with previous studies. Changes in the ambient ions (such as ammonium, sulfate, nitrate, chloride, and nitrite in the particle- and gas- phase) and aerosol properties (e.g., aerosol water content, aerosol pH) were also quantified and discussed. Moreover, we estimated the total carbon and climate-related species (e.g., CO_2, CH_4, N_2O, and BC) emissions and compared them with fire emission inventories. Current biomass burning emission inventories have uncertainties in estimating small fire burned areas and emissions. For instance, we found that the Global Fire Assimilation System (GFAS) may underestimate emissions (e.g., CO) of this small wildfire while other inventories (GFED and FINN) showed significant overestimation. Considering that it is the first time to record wildfire plumes in this region, related atmospheric implications are presented and discussed.

Keywords

Wildfire; Air Quality; Emission Factor; Emission Inventory; VOLTAIRE Supersite.

Highlights

1. Young wildfire plumes were observed and documented for the first time in suburban Orléans city, France.

2. Regional air quality was reduced by the wildfire emissions.

3. Emission factors of various pollutants were derived and compared with the literature.

4. Current biomass burning emission inventories have uncertainties in estimating small fire emissions.

1 Introduction

The frequency of wildfire events as well as the extent of the burned areas shows an increasing trend globally due to climate change (Artés et al., 2019; Barbero et al., 2015; Liu et al., 2010; Randerson et al., 2012). During the combustion of biomass, numerous pollutants, including particles and gases, are emitted into the atmosphere, which could have potential impacts on air quality and global climate (Andreae, 2019; Jaffe and Wigder, 2012; Jost et al., 2003; Randerson et al., 2012).

On a regional scale, the emitted pollutants could exacerbate air pollution downwind of the wildfire. For instance, David et al. (2021) found that wildfire events in the US significantly enhanced the nationwide particulate matter with aerodynamic diameters smaller than 2.5 or 10 μm ($PM_{2.5}$ and PM_{10}). Considering that the number and severity of wildfire events are increasing, they suggested that wildfire impacts should be considered in the national ambient air quality standards and implementations. Besides, the emitted pollutants also affect ground-level O_3 (Jaffe and Wigder, 2012). As a secondary pollutant, O_3 could be consumed or accumulated within a biomass burning (wildfire) plume varying from different aging stages. In a very fresh plume, O_3 is typically consumed regarding its rapid reaction with the emitted NO. It is also possible that in the very early stages of plume formation, highly reactive organic molecules may serve to suppress ozone concentrations. As the plume is diluted and transported, O_3 can be produced through chemical reactions involving volatile organic compounds (VOCs) and NO_x ($NO + NO_2$) under sunlight irradiation (Granier et al., 2000; Jaffe and Wigder, 2012). For example, Wang et al. (2021) observed 10-40 ppbv O_3 enhancement at 30 km downwind of a wildfire in the US. In addition, when the plumes (typically VOC-rich) mix into urban plumes (typically NO_x-rich) substantial enhancement in O_3 formation is observed, which deteriorates urban air quality (Xu et al., 2021).

Carbon monoxide (CO) is considered to be the second-largest primary carbon compound (after carbon dioxide, CO_2) emitted from the wildfire processes, which accounts for nearly half of its global emissions (Zheng et al., 2019). CO is typically treated as a tracer for incomplete combustion, including biomass burning. The tropospheric lifetime of CO against OH with a

global mean of 1.5×10^6 molecules cm^{-3} (Seinfeld and Pandis, 2016) is about 5 weeks, implying that its concentration in the wildfire plume is dominated by the downwind dilution during transport over one week or so. Hence, the Emission factor ($EF(X)=\Delta X/\Delta CO$, where X represents the target species) of O_3 obtained in the wildfire plume was usually used for estimating the plume age (Jaffe and Wigder, 2012). Generally, its values were reported to be negative in a fresh wildfire plume and turned positive and increased progressively with the plume age (Jaffe and Wigder, 2012).

In addition to the long-lived greenhouse gases (GHGs, e.g., CO_2, CH_4, N_2O), non-methane hydrocarbons (NMHCs) could also be emitted from wildfires. Due to their high reactivity (with OH, O_3, or NO_3), NMHCs play important role in the in-plume photochemistry to produce secondary pollutants like particulate matter (PM), O_3, and other photo-oxidants. Furthermore, numerous NMHCs are toxic and the increase in their ambient concentration levels constitutes a risk to public health. To quantify their emissions from wildfires, their emission factors can be calculated (Andreae, 2019; Jost et al., 2003).

On a global scale, wildfires are an important GHG source (Friedlingstein et al., 2020; Saunois et al., 2020). Saunois et al. (2020) have estimated 17 Tg CH_4 yr^{-1} emissions from wildfire emissions from 2008 to 2017, which represents 5% of the total anthropogenic CH_4 emissions. In addition to GHGs emissions, depending on their size and location, wildfire plumes can be transported to the upper troposphere-lower stratosphere (UTLS) region, and hence, impact the global climate and stratospheric ozone layer (Baray et al., 2012; Hirsch and Koren, 2021; Hooghiem et al., 2020; Kloss et al., 2021, 2019; Yu et al., 2019). For example, Hirsch and Koren (2021) reported a record-breaking aerosol level in the stratosphere over the southern hemisphere caused by the intensive Australian bushfires. This wildfire smoke could have a lifetime of days to months, which allows the smoke to be uniformly mixed over most of the southern hemisphere, leading to a significant cooling effect of 1.0 ± 0.6 W m^{-2}.

Satellite observations can be used for estimating the burned area and emissions of wildfires. However, scaling this to small fires remains challenging (Ramo et al., 2021; Saunois et al., 2020). For instance, Ramo et al. (2021) found that the Moderate Resolution Imaging Spectroradiometer (MODIS) images underestimated the burned area of small fires (<100 ha) by 94% in sub-Saharan Africa. Hence, the regional impact on air quality and/or the global impact on climate from both small and large fires should be studied (Ramo et al., 2021), in particular in

those regions where few fire events were recorded. Herein, in the middle of September 2020, a wildfire occurred in southern Orléans city where few wildfire events have occurred in the past. To the best of our knowledge, no study has been conducted to quantify the impacts of wildfires on the air quality in this region. Based on atmospheric measurements along with trajectory model simulations, the impact of this wildfire on the air quality in suburban Orléans was quantified. Emissions of this wildfire were evaluated and compared with the fire emission inventories. Atmospheric implications are presented after analysis and discussion of the field measurements and model simulations.

2 Methods

2.1 The Sologne Forest Fire Event

At 15:44 (local time, UTC+2) on 14th September 2020, firemen in Orléans received the information about the fire in the Sologne forest (47.3726°N, 2.12987° E, Figure 1). Its spread was controlled but it was still active at 2:31 on 15th September (information obtained from Firefighters Loire-et-Cher, https://sdis41.fr/, last access: 17 January 2022). On 22nd September, the fire was considered permanently extinguished. In total, about 36.3 hectares of forests (vegetation above ground: coniferous trees, mainly Laricio pines; surface vegetation: heather, moors, etc.) were burned during this event.

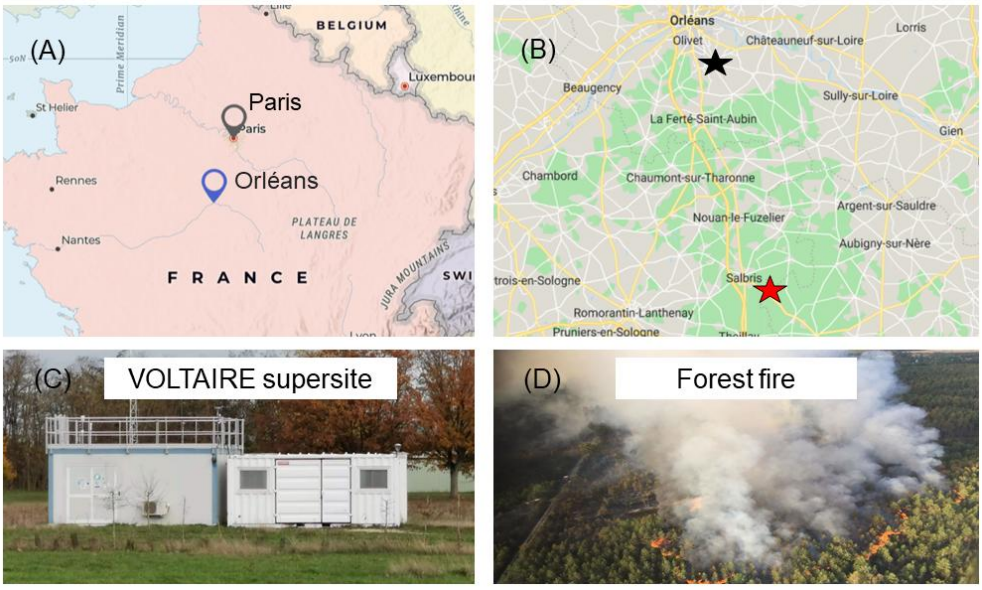


Figure 1. (A): Locations of Paris and Orléans (obtained from https://www.arcgis.com/, last access: 25 February 2022); (B): Locations of the forest fire (red star) and the VOLTAIRE

supersite (black star). Map base: © Google Map. (C) Photo of the VOLTAIRE supersite (© Chaoyang Xue); (D): Photo of the fire (© SDIS41).

2.2 Measurement Site and Instrumentation

Measurements used in this study were conducted at the VOLTAIRE supersite. It is located on the campus of the Centre National de Recherche Scientifique (CNRS, 47.8377º N, 1.9445º E) which is about 10 km south from Orléans city center and about 120 km southwest from Paris (Figure 1). Details about this station can be found in previous studies based on measurements at this site (Cai et al., 2022; Jiang et al., 2017).

At this site, NO_x ($NO + NO_2$), O_3, and meteorological parameters (temperature, pressure, relative humidity, solar radiation, wind speed, and wind direction) are continuously measured by a chemiluminescence technique (Model 42i, Thermo Fisher Scientific), a UV photometric analyzer (Model 49i, Thermo Fisher Scientific), and an auto meteorological station (Model CR800, Campbell Scientific), respectively. VOCs were measured online by a gas chromatographic (GC) system (airmoSCAN XPERT, Chromatotec®), with two different separation columns and three detectors (two flame ionization detectors and one quadrupole mass spectrometer). CO, NO_2, CH_4, and N_2O were measured by a three-channel infrared absorption spectrometer with quantum cascade lasers named SPIRIT, with a time resolution of 1.6 s (Brocchi et al., 2019; Catoire et al., 2017; Krysztofiak et al., 2018). Particulate matter was measured by an aerosol spectrometer Fidas® 200 (Palas®, Germany), analyzing ambient air in the size range of 180 nm – 18 µm (recording on PM_1, $PM_{2.5}$, PM_4, and PM_{10}). A URG-9000D Ambient Ion Monitor (AIM) was operated to measure gaseous pollutants (acetate, formate, NH_3, HONO, etc.) and PM_{10} composition (Cl^-, NO_3^-, SO_4^{2-}, NH_4^+, Na^+, K^+, etc.). Black carbon (BC) was measured by a black carbon monitor (Magee Scientific Aethalometer® Model AE33), which also includes the aethalometer model to quantify the contributions of wood-burning (BCwd) and fossil fuel (BCff) (Herich et al., 2011).

2.3 Models

The Lagrangian transport and diffusion model, FLEXible PARTicle (FLEXPART) v10.4, was used to calculate back trajectories of air masses reaching our measurement site (Brocchi et al., 2018; Pisso et al., 2019). The model simulation was based on ERA5 reanalysis data (grid resolution: 0.25º×0.25º, https://www.ecmwf.int/en/forecasts/datasets/reanalysis-datasets/era5,

last access: 17 January 2022) from European Center for Medium-range Weather Forecasts (ECMWF, https://www.ecmwf.int/, last access: 17 January 2022) was used for FLEXPART simulations (Hersbach et al., 2020). To obtain the trajectory frequency in the whole of September 2020, the HYbrid Single-Particle Lagrangian Integrated Trajectory Model (HYSPLIT, https://www.ready.noaa.gov/HYSPLIT.php, last access: 17 January 2022) was used.

To estimate the aerosol pH, an aerosol thermodynamic model, ISORROPIA II, (http://nenes.eas.gatech.edu/ISORROPIA/index_old.html, last access: 17 January 2022), was used (Fountoukis and Nenes, 2007). The model was run based on the AIM data (particle- and gas-phase), temperature, and relative humidity.

2.4 Inventories

Data from three fire emission inventories were used in this study. The Global Fire Assimilation System (GFAS, https://www.ecmwf.int/en/forecasts/dataset/global-fire-assimilation-system, last access: 17 January 2022) can provide daily emissions with a spatial resolution of 0.1˚×0.1˚ (Di Giuseppe et al., 2018). The FINN inventory (Fire INventory from NCAR) was developed by Wiedinmyer et al. (2011), and the data is available at https://www2.acom.ucar.edu/modeling/finn-fire-inventory-ncar (last access: 17 January 2022). Here we used a file configuration of FINNv2.4 with fire count of MODIS+VIIRS or MODIS, year of 2020, and speciation of GEOS-Chem. Daily emissions with a horizontal resolution of 1km are provided by this inventory. The GFED inventory (Global Fire Emissions Database, GFED4.1s, https://www.globalfiredata.org/, last access: 17 January 2022) developed by Van Der Werf et al. (2017) was also used in this study. It has a spatial resolution of 0.25˚×0.25˚. Monthly emissions with daily fractions are provided in this inventory. In addition, both GFAS and GFED inventories use emission factors from Andreae and Merlet (2001) and its corresponding update (Andreae, 2019) while the FINN inventory uses emission factors from Akagi et al. (2011).

3 Results and Discussion

3.1 General Overview of the Measurements

All the observations in the whole of September 2020 are presented and overviewed here to represent the typical meteorological and air quality conditions, while detailed analysis was

mostly focused on the wildfire plume and its comparison with measurements at the same hours on other days of September.

3.1.1 Meteorological Conditions

During the measurement period, it was mostly sunny and cloud-free except for a limited number of days (5th – 6th Sept. and 28th Sept. – 1st Oct.) when it was rainy or cloudy as reflected by the measured photosynthetically active radiation (PAR, Figure 2). The air temperature was typically around 20 ºC except for the last week (25th Sept. – 1st Oct.) when the temperature decreased to around 10 ºC caused by a cold front. The campaign-averaged temperature is 18.0 ± 6.0 ºC, respectively (Table 1). Throughout the campaign, air masses observed at this site originated from various directions (but few from South/Southeast/East), as reflected by the wind rose plot (Figure S1A) and the trajectory frequencies obtained from the HYSPLIT model (Figure S1B). Wind speed was generally less than 2 m s^{-1} except for the periods of 17th and from 23rd to 28th Sept. when the wind speed reached 4 m s^{-1}. The average wind speed was 1.3 ± 1.0 m s^{-1} during the campaign.

In particular, the highest temperature of 35.4 ºC and the lowest RH of 21.8% during the campaign occurred at 16:45 on 14th September, which is close to the occurrence of the forest wildfire. Daily average T of 22.6 ± 8.8 ºC and RH of 53 ± 22% on this day were the highest and lowest ones during the campaign, respectively. The wind direction was dominated by the south (the direction of the forest fire location) on the following day after the occurrence of the forest wildfire, which blew the emitted pollutants to the north of the fire, including the VOLTAIRE supersite.

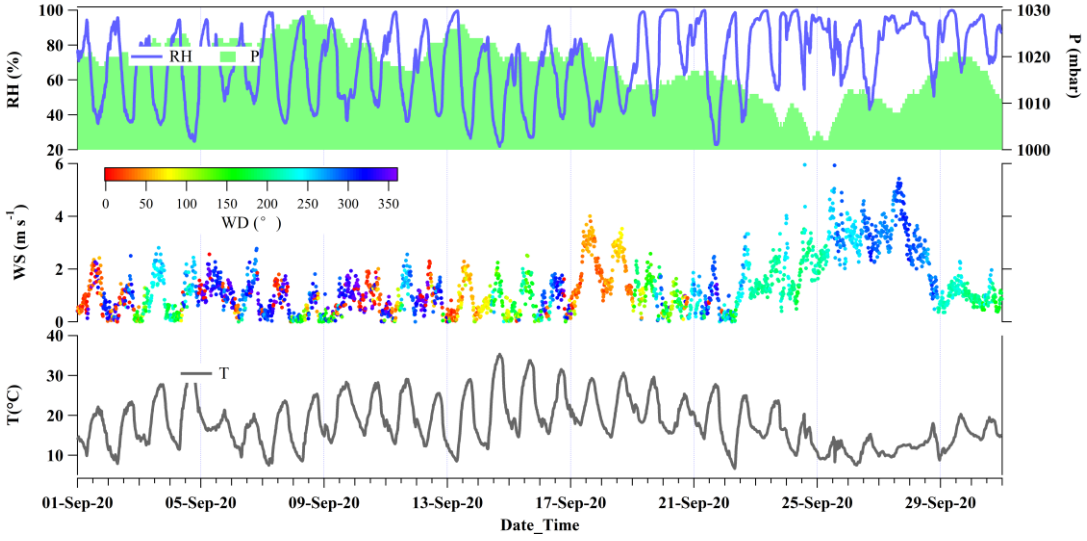


Figure 2: Meteorological parameters measured at the VOLTAIRE supersite. RH: relative humidity; P: pressure; WS: wind speed; WD: wind direction; T: temperature.

3.1.2 Pollutants

The VOLTAIRE supersite is located in a relatively clean area with the average $PM_{2.5}$ (6.7 μg m^{-3}), PM_{10} (12.8 μg m^{-3}), NO_2 (7.4 μg m^{-3}), and O_3 (63.6 μg m^{-3}) being lower than the World Health Organization (WHO) air quality guideline values (see WHO website: https://www.who.int/news-room/fact-sheets/detail/ambient-(outdoor)-air-quality-and-health, last access: 7 March 2022) of 15 μg m^{-3} (24 h mean) for $PM_{2.5}$, 45 μg m^{-3} (24 h mean) for PM_{10}, 25 μg m^{-3} (24 h mean) for NO_2, and 100 μg m^{-3} (8 h daily maximum) for O_3. All the pollutants exhibited much lower values during the period from 23rd to 28th Sept., as a result of fast dilution caused by high wind speeds (Figure 2).

Regarding the mass distribution of different particle sizes, average concentrations of PM_1, $PM_{1-2.5}$, $PM_{2.5-4}$, and PM_{4-10} were 5.0 ± 3.9, 1.7 ± 0.8, 1.6 ± 0.8, and 4.5 ± 3.7 μg m^{-3} (Table 1), with their contributions of 39%, 13%, 13%, and 35% to PM_{10}, respectively. BC was generally lower than 2 μg m^{-3}, with an average of 0.6 ± 0.4 μg m^{-3}. Significant enhancements in PM and BC were found in the wildfire plume observed on the morning of 15th Sept. and more analysis is presented in Section 3.2.

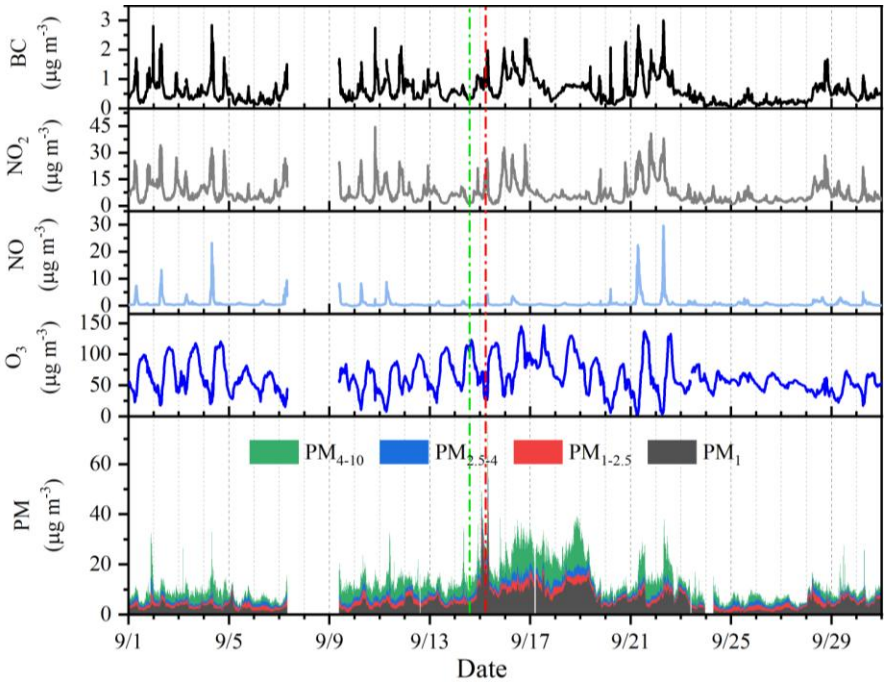


Figure 3: Time series of pollutants (PM, O_3, NO, NO_2 and BC, in µg m^{-3}) concentrations at the VOLTAIRE supersite (data from Lig'Air, https://www.ligair.fr/, last access: 7 March 2022). The green and red vertical lines indicate the occurrence of the forest fire in Souesmes and the observation of the wildfire plume at the VOLTAIRE supersite.

Table 1: Statistic description of the observations at the VOLTAIRE supersite during the whole of September 2020. Except for the meteorological parameters, all the pollutants listed in this table are in µg m^{-3}. For AIM data, p and g represent particle- or gas- phases, respectively.

Parameters	Average	Range	Parameters	Average	Range
T (ºC)	18.0±6.0	6.6-35.4	Sulfate (p)	1.1±0.5	≤2.9
PAR (µmol m^{-2} s^{-1})	17.7±24.2	0-91.2	Ammonium (p)	1.0±0.4	0.3-2.2
WS (m s^{-1})	1.3±1.0	0-5.9	Calcium (p)	0.3 ± 0.3	≤2.6
RH (%)	70.6±21.0	21.8-100	Magnesium (p)	0.04±0.03	≤0.19
P (mBar)	1018±5.9	1001-1030	Potassium (p)	0.2±0.1	≤0.8
BC	0.6±0.4	≤3.0	Sodium (p)	0.8±0.3	0.6-2.1
NO	0.8±1.9	≤29.7	Acetate (g)	2.4±1.3	0.7-7.4
NO_2	7.4±6.1	0.9-44.6	Formate (g)	1.1±0.9	0.1-4.1
O_3	63.6±26.5	2.4-146.4	Chloride (g)	0.19±0.14	0.05-0.90
PM_1	5.0±3.9	0.6-42.1	Nitrate (g)	0.4±0.2	≤1.1
$PM_{1-2.5}$	1.7±0.8	0.4-9.0	Nitrite (g)	0.7±0.6	0.1-4.4
$PM_{2.5-4}$	1.6±0.8	0.3-7.8	Sulfate (g)	0.5±0.8	≤4.9
PM_{4-10}	4.5±3.7	0.1-22.9	Ammonium (g)	2.7±1.4	0.1-4.4
Acetate (p)	$(8.7\pm2.8)\times10^{-4}$	≤0.002	Calcium (g)	0.04±0.02	0.01-0.16
Formate (p)	$(23\pm8.4)\times10^{-3}$	≤0.04	Magnesium (g)	$(1.8\pm1.4)\times10^{-3}$	≤0.02
Chloride (p)	0.13±0.21	≤1.2	Potassium (g)	0.12±0.07	≤0.36
Nitrate (p)	0.5±0.5	≤3.0	Sodium (g)	0.08±0.06	0.03-0.31
Nitrite (p)	0.02±0.01	≤0.06			

Ambient ions in the particle or gas phase are presented in Figure 4. In terms of the measured concentrations, sodium and ammonium were the most important cations in the particle phase, while nitrate and sulfate were the most important anions. On average, concentrations of sodium, ammonium, nitrate, and sulfate were 0.8±0.3, 1.0±0.4, 0.5±0.5, and 1.1±0.5 µg m^{-3} (Table 1),

with their mass contributions of 19.9%, 24.8%, 13.0%, and 25.9% to the total particle-phase ions (Figure S2), respectively. In contrast, the measured organics (acetate and formate), chloride, nitrite, calcium, magnesium, and potassium showed much lower levels, with a sum of their contributions of 16.4%. In the gas phase, the dominant ions were ammonium (33.2%), acetate (28.6%), formate (13.6%), nitrite (8.6%), and sulfate (6.1%) while contributions of other ions were all less than 5% (Figure S2).

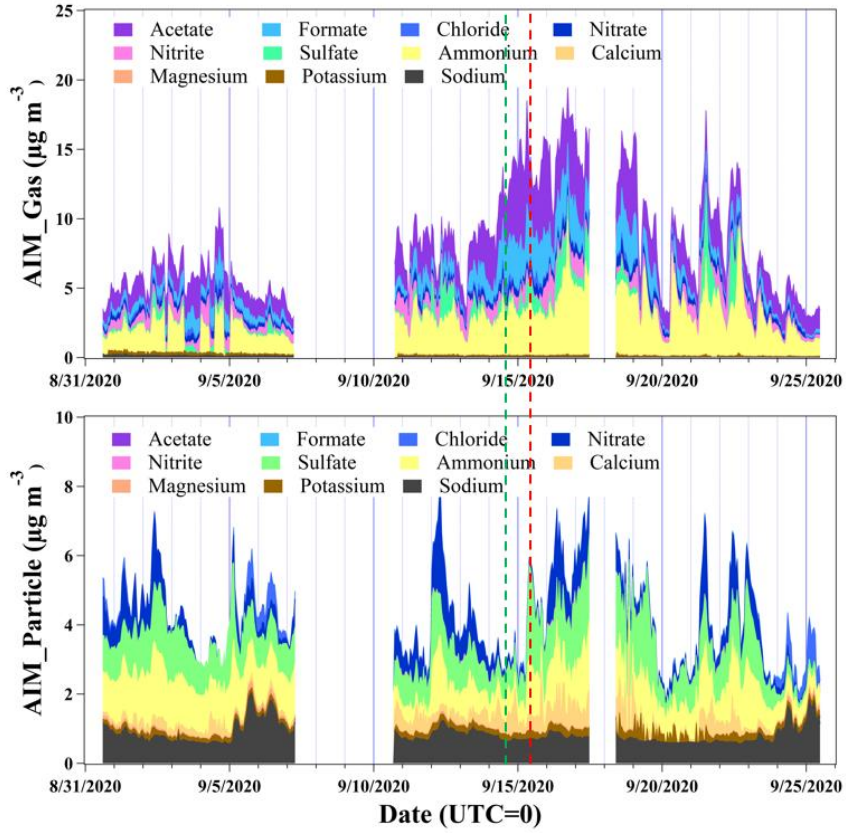


Figure 4: Gas- (upper panel) and particle-phase compositions of PM_{10} (lower panel) measured at the VOLTAIRE supersite. The green and red vertical lines indicate the occurrence of the forest fire in Souesmes and the observation of the wildfire plume at the VOLTAIRE supersite, respectively.

3.2 Observations of the wildfire Plume

Figure S3 shows the concentrations of CO, NO_2, CH_4, and N_2O measured by SPIRIT at the supersite. Stable measurements started at 9:27 on 15th September and the first measured CO concentration was 837 ppbv, which is much higher than the background level of around 100 ppbv. Later, the highest CO concentration of 1050 ppbv was observed at 09:38. High

concentrations of NO_2 (9.3 ppbv), N_2O (334 ppbv), and CH_4 (2203 ppbv) were also observed within 10 mins around the CO peak. Meanwhile, the levels of other measured pollutants (e.g., PM, BC, sulfate) showed a simultaneous increase (Figure 3 and Figure 4). For example, the PM_{10} level of 75.9 μg m^{-3} was the highest one in September and more than 6 times higher than the campaign average value of 12.7 μg m^{-3}, revealing the significant impact of this forest fire on the air quality in this region. In addition, a view from the satellite (Figure S4) also observed the wildfire and the regional spread of its emissions.

3.2.1 Emission Factors (EF)

As the forest fire occurred around 15:35 on 14th September and the wildfire plume was observed at 9:38 (local time, the occurrence of the CO peak) on 15th September, the plume age should be <18 h (from the trajectory a plume age <12 h could be obtained and mostly during night-time). Besides, a significant O_3 decrease by ca. 13 ppbv was observed in this wildfire plume indicating the plume did not undergo much photochemistry that could lead to O_3 production. For instance, Jost et al. (2003) found a significant O_3 enhancement in a wildfire plume after 2 h photochemistry. Hence, the wildfire plume observed here should be relatively fresh (also see the trajectory in Section 3.3). However, previous field and laboratory studies have reported the impact of near-source transformation on the properties of wildfire plumes, which may influence the EF values (Collier et al., 2016; Hodshire et al., 2019; Li et al., 2021). The derived EF values are focused on gas species, for which the atmospheric oxidization process may cause major uncertainties. Hence, we employed a method to constrain the uncertainties, which are generally caused by the chemical loss mainly through OH oxidization. Take toluene as an example, its reaction rate with OH is 5.6×10^{-12} cm^3 $molecule^{-1}$ s^{-1} at 298 K (Mellouki et al., 2021). Assuming a relatively high OH concentration of 5×10^5 molecule cm^{-3}, a negligible amount of CO but 11% of toluene will be lost through OH oxidization in 12 hours, leading to an underestimation by <11% in EF(toluene). Similarly, other EF uncertainties caused by the OH oxidization process can be estimated, which is summarized in the updated Table 2. Please note that we used a higher OH concentration to constrain the upper limit of the uncertainties.

Table 2: Emission factors (EF) inferred from the wildfire plume. Units: ppbv ppbv^{-1} for Efs of NO_2, CH_4, and N_2O (measured by SPIRIT); μg m^{-3} ppbv^{-1} for all the others. BTEX = Benzene + Toluene + Ethylbenzene + m/p/o -Xylenes. Comparisons with temperate forest fire summarized in Andreae (2019) were also shown. Note that the original values in Andreae (2019) are given in gram species per kilogram dry matter burned and they are converted to EFs for comparison. Atmospheric OH rate constants were taken from Mellouki et al. (2021) or Atkinson and Arey (2003).

X	EF (X)	Uncertainty %	R^2	Andreae (2019)
O_3	-4.9E-2		0.70	
NO	8.8E-4		0.47	2.5E-2
CH_4	2.3E-1		0.79	8.2E-2
N_2O	1.7E-2		0.84	1.4E-3
BC	2.8E-4		0.70	1.2E-2
123-TMB	7.8E-6	51	0.99	
124-TMB	1.7E-5	50	0.80	
135-TMB	2.7E-6	71	0.86	
BTEX	1.2E-4		0.62	2.5E-3
Ethylbenzene	1.6E-5	14	1.00	9.7E-5
Toluene	5.2E-5	11	0.90	7.5E-4
α-Pinene	1.3E-5	68	0.69	
n-Octane	8.7E-5	16	0.88	
n-Propylbenzene	7.5E-6	12	0.67	
p-Ethytoluene	3.5E-6	22	0.92	
m-Diethylbenzene	6.8E-7		0.45	
m-Ethyltoluene	6.2E-6	33	0.95	
methyl ethyl ketone	2.5E-4	35	0.35	
n-Decane	3.5E-6	21	1.00	

The molar enhancement ratio of compound X compared to CO was defined as EF(X)=ΔX/ΔCO (Andreae, 2019; Jost et al., 2003), which was used here to estimate the wildfire emissions. To avoid the uncertainty caused by the selection of background levels, we used the slope of the regression line between species X and CO as the EF (X) during the pollution case (Jost et al., 2003). Table 2 shows the derived EFs and the correlations for numerous species. As mentioned before, a decreased O_3 resulted in a negative EF(O_3) of -0.05 μg m^{-3} $ppbv^{-1}$ (equivalent to -0.026 ppbv $ppbv^{-1}$) was obtained here, indicating a young wildfire plume. Most correlation coefficients are high, implying that the increase in species X and CO are caused by the same source, the wildfire plume. Poor correlations between some species (e.g., xylenes, benzene) and CO are also found, which might be caused by the complexity of the emissions as well as the ambient dilution process. In particular, significant CH_4 emission reflected by a high CH_4 peak of 2203 ppbv and a positive EF(CH_4) of 0.23 ppbv $ppbv^{-1}$ was found in this wildfire plume, implying the burning of the herbaceous layer (Andreae, 2019; Jost et al., 2003). This may also explain the higher EF(CH_4) and EF(N_2O) obtained here than those from the averages of temperate forest fires (0.08 and 0.001 ppbv $ppbv^{-1}$, respectively) (Andreae, 2019). Other EFs are lower than those from temperate fires (Andreae, 2019), indicating the potential impact of dilution and highlighting the complexity of the wildfire emissions and their impacts on ambient pollutant levels. Although this fire was small (36.3 ha burned area) compared with the fires summarized in Andreae (2019), it has been suggested that the relatively high EFs for greenhouse gases (N_2O and CH_4) from small fires may be of importance to the global greenhouse gas budget (Randerson et al., 2012).

3.2.2 Impacts on BC and Particle Size Distribution

We explored the possible impact of this forest fire, even though a small one, on the measured BC levels and its sources. Figure 5 shows the average concentration of measured BC_{wb} (BC derived from wood burning) and BC_{ff} (BC derived from fossil fuel) in the wildfire plume or non-wildfire plumes at the same hours (9:00-11:00). BC_{ff} was the major source for the measured total BC at this site and about one order of magnitude higher than BC_{wd} in non-wildfire plumes. Considering that the measurements covered rush hours, the source of BC in non-wildfire plumes was attributed to fossil fuel combustion. The corresponding BC_{wb}/BC_{ff} ratio of 0.08 was in the range of 0.02 – 0.11 reported in other sites in Europe during summertime (Herich et al., 2011). However, BC_{wd} increased significantly in the wildfire plume (0.3±0.19 μg m^{-3}, non-wildfire plume: 0.06±0.05 μg m^{-3}) while BC_{ff} kept a similar level (0.95±0.38 μg m^{-3}) to that in non-

wildfire plumes (0.77±0.57 μg m^{-3}), leading to an increasing BC_{wb}/BC_{ff} ratio of 0.32, which is in the range of values (0.3 – 0.5) impacted by wildfire emissions (Helin et al., 2018; Herich et al., 2011; Kalogridis et al., 2018; Yttri et al., 2014). This indicates the potential impact of this wildfire on regional BC levels.

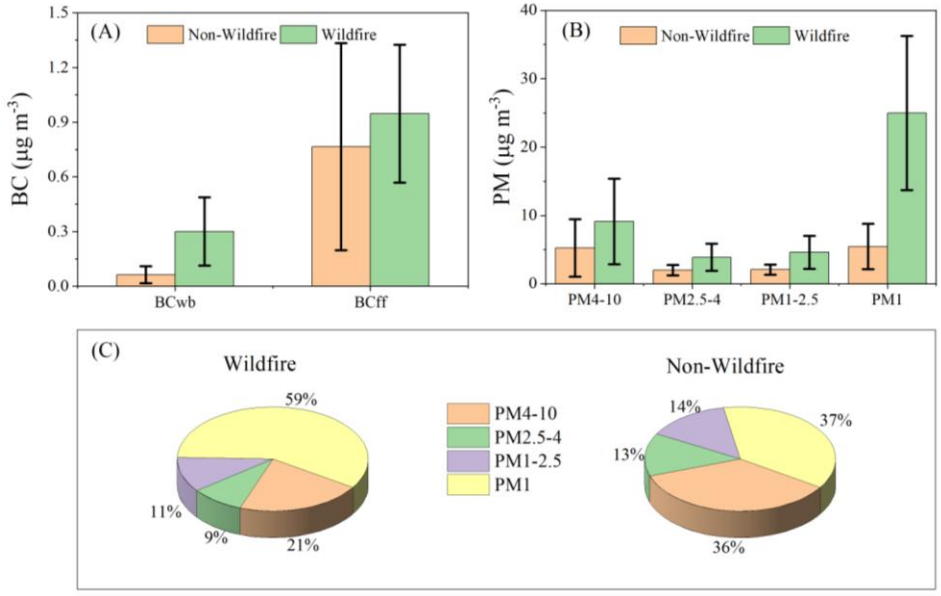


Figure 5: Levels of (A) BC_{wb} and BC_{ff}, and (B) PM at different sizes, and (C) their relative mass contributions of different PM sizes to PM_{10} in the wildfire or non-wildfire plumes during the same hours (9:00 – 11:00) considering that the detection of the plume covered rushing hours.

Figure 5B and C show PM mass concentrations at different sizes (PM_1, $PM_{1\text{-}2.5}$, $PM_{2.5\text{-}4}$, and $PM_{4\text{-}10}$) and their relative contributions in the wildfire or non-wildfire plumes during the same hours (9:00 – 11:00). Average $PM_{2.5}$ (or PM_{10}) in the non-wildfire plumes during the same hours of the day was 7.5 (or 14.7) μg m^{-3}, which is much lower than the WHO air quality guideline $PM_{2.5}$ (or PM_{10}) value of 15 (or 45) μg m^{-3} (24 h mean). However, in the wildfire plume, the average $PM_{2.5}$ (or PM_{10}) increased to 29.6 (or 42.6) μg m^{-3}, which exceeds (or becomes close to) the WHO air quality guideline $PM_{2.5}$ (or PM_{10}) value, indicating a potential public health risk caused by wildfire emissions (PM, BC, VOCs, etc.). Moreover, wildfire emissions can cause changes in particulate size distribution. For instance, mass concentrations of PM_1, $PM_{1\text{-}2.5}$, $PM_{2.5\text{-}4}$, and $PM_{4\text{-}10}$ in the non-wildfire plumes were 5.5, 2.1, 2.0, and 5.2 μg m^{-3}, with relative contributions of 37%, 14%, 13%, and 36%, respectively. All their mass concentrations showed a significant increase (from 5.5 to 25.0, 2.1 to 4.6, 2.0 to 3.9, and 5.2 to 9.1 μg m^{-3} for PM_1, $PM_{1\text{-}}$

$_{2.5}$, $PM_{2.5-4}$, and PM_{4-10}, respectively), while their contributions changed remarkably within the biomass burning plume, particularly PM_1 and PM_{4-10} whose contributions increased to 59% or decreased to 21%, respectively. As reported in previous studies, wildfire can emit various sizes of particles. However, particles with a smaller diameter (i.e., submicron particles) hold a relatively longer atmospheric lifetime against deposition so that they may undergo a regional transportation process (Gallagher et al., 2002).

3.2.3 Impacts on Ambient Ions in the Particle- and Gas-Phase

Figure 6A displays the relative mass contribution of each particle-phase cation or anion to their total masses. During the non-wildfire period, anions were dominated by SO_4^{2-} and NO_3^-, with contributions of 49% and 40%, respectively. Within the young wildfire plume, SO_4^{2-} was enhanced from 1.1 to 2.3 μg m^{-3} while NO_3^- reduced from 0.9 to 0.2 μg m^{-3}, resulting in a dominant role of SO_4^{2-} (89%) in the total particle anion mass. NH_4^+ and Na^+ were the two most important cations in the particle phase with contributions of 45% and 34% in the non-wildfire plumes, respectively, which is similar to other European locations (Tang et al., 2021). NH_4^+ was slightly enhanced from 1.2 to 1.4 μg m^{-3} while Na^+ slightly decreased from 0.9 to 0.7 μg m^{-3} in the wildfire plume compared to the non-wildfire plumes, leading to a larger NH_4^+ contribution of 51%.

Figure 6B shows the relative mass contribution of each gas-phase cation or anion to their total masses. The gas-phase anions are typically in their acid forms, i.e., the measured gas-phase $HCOO^-$, CH_3COO^- and NO_2^- were in the form of HCOOH, CH_3COOH, and HONO in the atmosphere, respectively. A remarkable increase in organic acids (CH_3COOH and HCOOH) was found within the wildfire plume. Their concentrations increased from 2.0 to 5.7 or from 1.2 to 3.7 μg m^{-3}, respectively, suggesting strong emissions of organic acids from the wildfire (Burling et al., 2010; Chaliyakunnel et al., 2016; R'Honi et al., 2013). Interestingly, significant gas-phase SO_4^{2-} (i.e., H_2SO_4) enhancement was also found within this wildfire plume as its concentration increased from 0.8 μg m^{-3} to 1.7 μg m^{-3}, which may have an impact on sulfate aerosol formation and new particle formation.

No apparent enhancement of HONO (gas-phase NO_2^-) was observed in the wildfire plume, contrary to previous studies (e.g., Nie et al., 2015; Peng et al., 2020; Theys et al., 2020), which presented significant HONO emissions from biomass burning process. Although this does not preclude the possibility of HONO emissions from the fire since HONO concentrations will be

affected by dilution and photochemical loss processes (Wang et al., 2021). Gas-phase cation NH_4^+ (in the form of NH_3) predominated, with a concentration of 3.1 and 3.5 μg m^{-3} in the non-wildfire and wildfire plumes, respectively, which is comparable to other European cities (Tang et al., 2021).

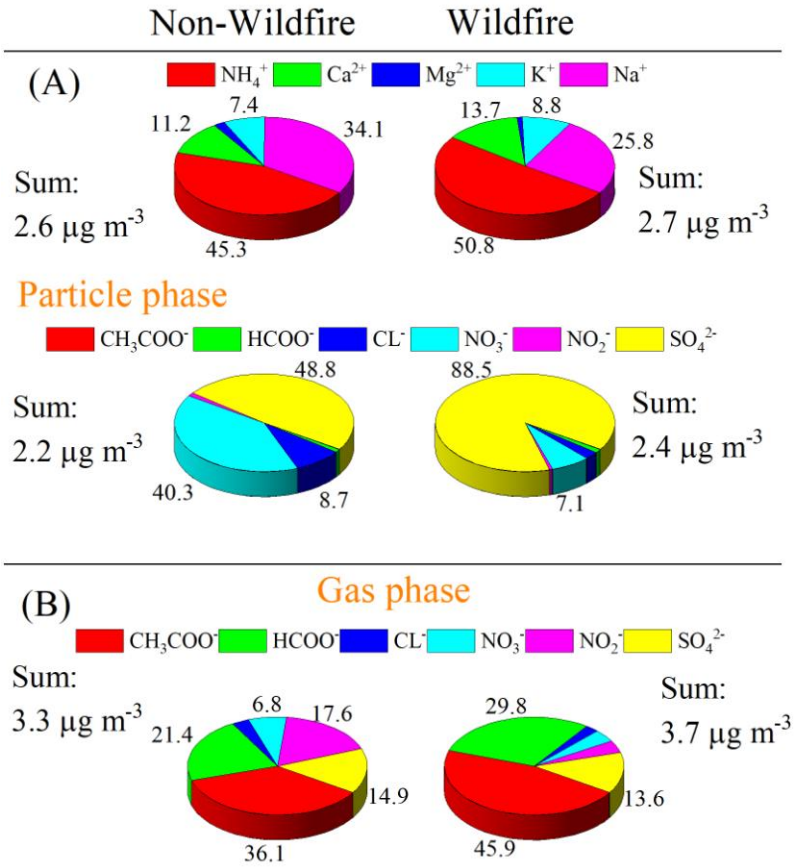


Figure 6: Relative contributions (%) of each cation/anion in the particle-phase (A) and gas-phase (B) masses. Percentages less than 5% were not shown. In the gas-phase, concentrations of the only cation source, NH_3, are 3.1 and 3.5 μg m^{-3} during non-wildfire and wildfire periods, respectively.

3.3 Emission Estimation and Comparison with GFAS

3.3.1 FLEXPART Simulations

Figure 7 illustrates the 12-h back trajectory (starting from CO peak at 9:38 local time) obtained from the FLEXPART simulation. It was found that the air mass at the VOLTAIRE supersite mainly originated from the south and southwest, which is consistent with the wind measurements at this station on 14th and 15th September (Figure 2). Some clusters originated from the area

above the wildfire (Figure 7). Hence, the large increase in pollutants, such as CO from ~100 ppbv to 1050 ppbv, is attributed to the transportation of the wildfire plume. The satellite also captured the widespread plumes (Figure S4), indicating the impacts of wildfire emissions on regional air quality. Besides, quantification of emissions from this wildfire is of significance for understanding the role and impacts of small wildfires on regional air quality and global climate.

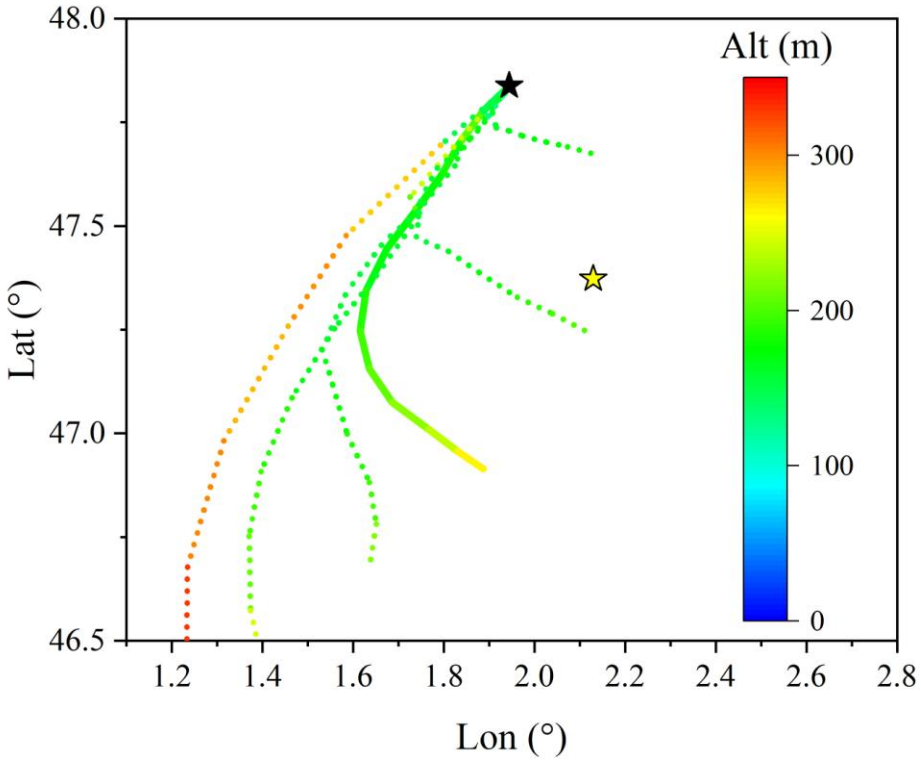


Figure 7: FLEXPART back trajectory with clusters. The black and the yellow stars represent the locations of the VOLTAIRE supersite and the wildfire.

3.3.2 Emission Estimation vs. GFAS vs. GFED vs. FINN

We estimated carbon emissions from this fire event and compared them with current biomass burning inventories. A standard equation, developed by Seiler & Crutzen (1980), was popularly used for calculating the total carbon emission from a forest fire (C_{total}).

$$C_{total} = A * B * f_c * \beta, \quad \text{(Eq-1)}$$

where A, B, f_c, and β represent the total burned area (36.3 ha), biomass density (t ha^{-1}), the fraction of carbon of the biomass, and the fraction of carbon consumed during the burning process, respectively. Considering the composition differences, such as organic mat on the forest

floor and in peatlands, components on the ground layer and above the ground layer are estimated separately. French et al. (2002) furtherly modified the equation to:

$$C_{total} = A * (B_a * f_{ca} * \beta_a + C_g * \beta_g), \quad \text{(Eq-2)}$$

where B_a, f_{ca}, β_a, C_g, and β_g denote the average biomass density of the above vegetation (t ha^{-1}), the carbon fraction of the aboveground biomass with an assumed value of 0.50, the fraction of the aboveground biomass consumed during the fire, the carbon density (15 t-C ha^{-1} from French et al. (2002)) of the organic mat exposed to the fire, and the fraction of the organic mat consumed during the fire, respectively. B_a was set as 50 t ha^{-1} obtained from the European Space Agency BIOMASS mission (Quegan et al., 2019). 50-year average values of β_a (0.33) and β_g (0.25) for forest fires obtained from French et al. (2002) were adopted in this calculation. Then we obtained the C_{total} of 435.6 t for this forest fire. This leads to an average carbon emission of 12 t-C ha^{-1}, which is comparable to previous studies of 5 – 40 t-C ha^{-1} (French et al., 2002; Randerson et al., 2012).

Emission factors of CO_2, CO, and CH_4 during flaming (EF_f, kg gas (g total carbon)$^{-1}$) and smoldering (EF_s, kg gas (g total carbon)$^{-1}$) periods were taken from French et al. (2002) in which they calculated the average of values reported by several previous studies (Table S1). For emission factors of BC and N_2O, the derived Emission factors in Table 2 were used. As shown in Table 3, the calculated emissions of CO_2, CO, CH_4, BC, and N_2O were 1370 (1128), 82.8 (200), 2.4 (6.6), 0.017 (0.048), and 0.019 (0.054) t (unit: ton), assuming the fire was always at the flaming (or smoldering) stage, respectively. Note that the actual emission should be between those two numbers as a wildfire event typically undergoes both flaming and smoldering stages.

For the GFAS inventory, emissions were only detected on 14th September, with a daily average of grid CO emission of 1.5×10^{-9} kg m^{-2} s^{-1}. The total CO emission based on the GFAS inventory was ca. 11 t. Similarly, the GFAS-derived total carbon, CO_2, CH_4, N_2O, and BC emissions from this wildfire were about 161.4, 1.0, 0.01, 0.05 t, respectively. All the GFAS-derived emissions except for BC and N_2O were much lower than the estimated ones, either M_f or M_s.

GFED and FINN inventories captured the wildfire on both 14th and 15th. However, the burned area in the FINN inventory is largely overestimated, either for fire counted by MODIS (175.5 ha) or MODIS+VIIRS (270.6 ha). This leads to larger emissions such as total carbon of 2210.7 (1455.6) t, CO_2 of 7283.8 (4791.0) t, CO of 493.3 (328.0) t, etc. in FINN with fire counted by MODIS+VIIRS (or by MODIS only). Likewise, for the GFED inventory, similar emission levels

of total carbon (2553.8 t), CO_2 (8554.2 t), CO (475.2 t), and CH_4 (20.2 t) were obtained. However, emissions of BC (2.9 t) and N_2O (0.77 t) from the GFED inventory are much higher than others.

Table 3: Emission factors during flaming (EF_f, g gas (kg total carbon)$^{-1}$) and smoldering (EF_s, kg gas (g total carbon)$^{-1}$) periods, and the total released mass of each gas/particle during the two periods (M_f and M_s, in t).

Emissions	Burned Area (ha)	C_{total} (ton)	CO_2 (ton)	CO (ton)	CH_4 (ton)	BC (ton)	N_2O (ton)
Estimation	36.3[a]	453.6	1128[s]-3145[f]	82.8[f] -200[s]	2.4[f]-6.6[s]	0.017[f]-0.048[s]	0.019[f]-0.054[s]
GFAS		53.1	161.4	11.0	1.0	0.05	0.011
GFED		2553.8	8554.2	475.2	20.2	2.9	0.77
FINN (MODIS+VIIRS)	270.6	2210.7	7283.8	493.3	17.0	0.035	
FINN (MODIS)	175.5	1455.6	4791.0	328.0	11.1	0.022	
FINN[c]	187.5	1560.9	5135.5	352.9	12.0	0.024	

[a]: obtained from Sapeurs-Pompiers Loire-et-Cher; [s]: smoldering period; [f]: flaming period. Note that differences between FINN (MODIS) and FINN (MODIS+VIIRS) were possibly caused by the fact that the fire was detected twice on 15th Sept. in FINN (MODIS+VIIRS), which can be obtained from Table S2; [b]: sum of carbon in the form of CO_2, CO, CH_4, and BC; [c]: using the average of the twice detection.

Previous studies reported underestimation of small fire emissions possibly due to the uncertainties in burned area estimation (Ramo et al., 2021; Saunois et al., 2020). In the present study, we found a similar underestimation by the GFAS inventory. In contrast, significant overestimation in the burned area, and total carbon, CO_2, CO, and CH_4 emissions were found in the GFED and the FINN inventories. Regarding the significant overestimation in the burned area, in general, the reason is that current inventories use a coarse spatial resolution, such as 0.25×0.25 for GFED. For the FINN inventory, the burned area was classified according to land cover. For instance, in our case, woody savanna/shrublands, temperate forest, and temperate evergreen forest were identified in the FINN inventory, then the burned area can be overestimated when summing up all the burned areas. As far as we know, a new version of the FINN inventory is forthcoming (https://www2.acom.ucar.edu/modeling/finn-fire-inventory-ncar, last access: 11 July 2022), which should improve the performance in estimating small fire

emissions. Hence, improvement of the inventory performance in small fire emissions is needed to quantify emissions of small fires and their environmental impacts. Differences between different inventories also suggest the necessary inter-comparison between inventories.

4 Conclusion and Implication

In the middle of September 2020, a forest wildfire occurred in the Sologne forest in Souesmes (Loir-et-Cher, Sologne, France) and its plume spread to 200 km in the following day, as observed by the MODIS satellite. At the VOLTAIRE supersite in suburban Orléans (about 50 km northwest of the wildfire location), instruments for various trace gases and particle compositions detected young biomass burning plumes from this wildfire. The data obtained enabled us to quantify the emissions from that fire and evaluate the possible impact on air quality in suburban Orléans.

Average concentrations of $PM_{2.5}$ and PM_{10} in September were 6.7 and 12.8 μg m^{-3}, respectively, which are close to or lower than the updated WHO air quality guideline values of 5 and 15 μg m^{-3}, respectively. However, $PM_{2.5}$ and PM_{10} levels in the periods that were affected by wildfire emissions increased substantially (29.6 and 42.6 μg m^{-3}, respectively) and exceeded the WHO air quality guideline values (Figure 3). Additionally, levels of a series of VOCs including BTEX were also enhanced by the wildfire event.

Besides, the impacts of the wildfire on the size, composition, and properties of aerosol were quantified. Within the wildfire plume, an increase in BC was observed and the observed BC_{wb}/BC_{ff} ratio of 0.32 was in the range of values (0.3 – 0.5) impacted by wildfire emissions. Aerosol pH was significantly reduced in the plume as a result of the increase in sulfate. Besides, Emission factors compared to CO were calculated for various gaseous pollutants and compared with previous studies. Relatively higher EF ratios for GHGs (CH_4 and N_2O) were found within the plume from this wildfire, indicative of the possibly important role of small fires in GHGs burden.

Furthermore, emissions of this wildfire were estimated and compared with GFAS emission inventory. We found that the GFAS emission inventory significantly underestimated the emission from this small fire, which agrees with other studies (Ramo et al., 2021; Wang et al., 2021). This study suggested that the detection and prediction of small fire emissions still need further assessment and improvement.

The year 2020 was a warm year in Europe, with the autumn having the highest recorded temperatures since 1950 (see ECWMF news at https://climate.copernicus.eu/esotc/2020/temperature, last access: 17 January 2022). Higher temperatures are expected to lead to wildfire events in wildfire hotspot regions as well as those regions where few wildfires were recorded before (e.g., Orléans) (Liu et al., 2010; Randerson et al., 2012), which may be exacerbated by climate change. This not only reduces regional air quality near those wildfires but also increases global greenhouse gas emissions. We suggest that besides the major wildfire regions, attention should also be paid to the regions with few wildfires recorded so far, in order to better understand their environmental effects and how their distribution may change over time.

Acknowledgments

We thank Ministère de l'Agriculture et de l'Alimentation for providing information (including the photo) about the wildfire.

Author Contribution

A.M. and V.C. led this study. C.X., B.G., Y.R., M.C., P.M., F.L.F., and C.R. performed the measurements. C.X. and G.K. performed the model simulations. C.X. took the lead in data analysis and manuscript writing with input from all co-authors. V.D., Y.M., MMG, A.M., and V.C. revised the manuscript. All authors discussed the results and approved the final manuscript.

Funding

This study was supported by the VOLTAIRE project (ANR-10-LABX-100-01) funded by the ANR and the PIVOTS project provided by the Region Centre − Val de Loire (ARD 2020 program and CPER 2015 − 2020).

Competing Interests

The authors declare no competing financial interest.

Data Availability

All the data presented in this study are available upon request from the corresponding authors.

References

Akagi, S.K., Yokelson, R.J., Wiedinmyer, C., Alvarado, M.J., Reid, J.S., Karl, T., Crounse, J.D., Wennberg, P.O., 2011. Emission factors for open and domestic biomass burning for use in atmospheric models. Atmos. Chem. Phys. 11, 4039–4072. https://doi.org/10.5194/acp-11-4039-2011

Andreae, M.O., 2019. Emission of trace gases and aerosols from biomass burning - An updated assessment. Atmos. Chem. Phys. 19, 8523–8546. https://doi.org/10.5194/acp-19-8523-2019

Andreae, M.O., Merlet, P., 2001. Emission of trace gases and aerosols from biomass burning. Global Biogeochem. Cycles 15, 955–966. https://doi.org/10.1029/2000GB001382

Artés, T., Oom, D., de Rigo, D., Durrant, T.H., Maianti, P., Libertà, G., San-Miguel-Ayanz, J., 2019. A global wildfire dataset for the analysis of fire regimes and fire behaviour. Sci. Data 6, 296. https://doi.org/10.1038/s41597-019-0312-2

Atkinson, R., Arey, J., 2003. Atmospheric Degradation of Volatile Organic Compounds. Chem. Rev. 103, 4605–4638. https://doi.org/10.1021/cr0206420

Baray, J.L., Duflot, V., Posny, F., Cammas, J.P., Thompson, A.M., Gabarrot, F., Bonne, J.L., Zeng, G., 2012. One year ozonesonde measurements at Kerguelen Island (49.2°S, 70.1°E): Influence of stratosphere-to-troposphere exchange and long-range transport of biomass burning plumes. J. Geophys. Res. Atmos. 117, 1–10. https://doi.org/10.1029/2011JD016717

Barbero, R., Abatzoglou, J.T., Larkin, N.K., Kolden, C.A., Stocks, B., 2015. Climate change presents increased potential for very large fires in the contiguous United States. Int. J. Wildl. Fire 24, 892–899. https://doi.org/10.1071/WF15083

Brocchi, V., Krysztofiak, G., Catoire, V., Guth, J., Marécal, V., Zbinden, R., El Amraoui, L., Dulac, F., Ricaud, P., 2018. Intercontinental transport of biomass burning pollutants over the Mediterranean Basin during the summer 2014 ChArMEx-GLAM airborne campaign. Atmos. Chem. Phys. 18, 6887–6906. https://doi.org/10.5194/acp-18-6887-2018

Brocchi, V., Krysztofiak, G., Deroubaix, A., Stratmann, G., Sauer, D., Schlager, H., Deetz, K., Dayma, G., Robert, C., Chevrier, S., Catoire, V., 2019. Local air pollution from oil rig emissions observed during the airborne DACCIWA campaign. Atmos. Chem. Phys. 19, 11401–11411. https://doi.org/10.5194/acp-19-11401-2019

Burling, I.R., Yokelson, R.J., Griffith, D.W.T., Johnson, T.J., Veres, P., Roberts, J.M., Warneke, C., Urbanski, S.P., Reardon, J., Weise, D.R., Hao, W.M., De Gouw, J., 2010. Laboratory measurements of trace gas emissions from biomass burning of fuel types from the southeastern and southwestern United States. Atmos. Chem. Phys. 10, 11115–11130. https://doi.org/10.5194/acp-10-11115-2010

Cai, M., Ren, Y., Gibilisco, R.G., Grosselin, B., McGillen, M.R., Xue, C., Mellouki, A., Daële, V., 2022. Ambient BTEX concentrations during the COVID-19 lockdown in a peri-urban environment (Orléans, France). Atmosphere (Basel). 13. https://doi.org/10.3390/atmos13010010

Catoire, V., Robert, C., Chartier, M., Jacquet, P., Guimbaud, C., Krysztofiak, G., 2017. The SPIRIT airborne instrument: a three-channel infrared absorption spectrometer with quantum cascade lasers for in situ

atmospheric trace-gas measurements. Appl. Phys. B 123, 244. https://doi.org/10.1007/s00340-017-6820-x

Chaliyakunnel, S., Millet, D.B., Wells, K.C., Cady-Pereira, K.E., Shephard, M.W., 2016. A Large Underestimate of Formic Acid from Tropical Fires: Constraints from Space-Borne Measurements. Environ. Sci. Technol. 50, 5631–5640. https://doi.org/10.1021/acs.est.5b06385

Collier, S., Zhou, S., Onasch, T.B., Jaffe, D.A., Kleinman, L., Sedlacek, A.J., Briggs, N.L., Hee, J., Fortner, E., Shilling, J.E., Worsnop, D., Yokelson, R.J., Parworth, C., Ge, X., Xu, J., Butterfield, Z., Chand, D., Dubey, M.K., Pekour, M.S., Springston, S., Zhang, Q., 2016. Regional Influence of Aerosol Emissions from Wildfires Driven by Combustion Efficiency: Insights from the BBOP Campaign. Environ. Sci. Technol. 50, 8613–8622. https://doi.org/10.1021/acs.est.6b01617

David, L.M., Ravishankara, A.R., Brey, S.J., Fischer, E. V, Volckens, J., Kreidenweis, S., 2021. Could the exception become the rule? "Uncontrollable" air pollution events in the U.S. due to wildland fires. Environ. Res. Lett. 16, 034029. https://doi.org/10.1088/1748-9326/abe1f3

Di Giuseppe, F., Rémy, S., Pappenberger, F., Wetterhall, F., 2018. Using the Fire Weather Index (FWI) to improve the estimation of fire emissions from fire radiative power (FRP) observations. Atmos. Chem. Phys. 18, 5359–5370. https://doi.org/10.5194/acp-18-5359-2018

Fountoukis, C., Nenes, A., 2007. ISORROPIA II: a computationally efficient thermodynamic equilibrium model for K+-Ca2+–Mg2+–NH4+–Na+–SO42−–NO3−–Cl−–H2O aerosols. Atmos. Chem. Phys. 7, 4639–4659. https://doi.org/10.5194/acp-7-4639-2007

French, N.H.F., Kasischke, E.S., Williams, D.G., 2002. Variability in the emission of carbon-based trace gases from wildfire in the Alaskan boreal forest. J. Geophys. Res. 108, 8151. https://doi.org/10.1029/2001JD000480

Friedlingstein, P., O'Sullivan, M., Jones, M.W., Andrew, R.M., Hauck, J., Olsen, A., Peters, G.P., Peters, W., Pongratz, J., Sitch, S., Le Quéré, C., Canadell, J.G., Ciais, P., Jackson, R.B., Alin, S., Aragão, L.E.O.C., Arneth, A., Arora, V., Bates, N.R., Becker, M., Benoit-Cattin, A., Bittig, H.C., Bopp, L., Bultan, S., Chandra, N., Chevallier, F., Chini, L.P., Evans, W., Florentie, L., Forster, P.M., Gasser, T., Gehlen, M., Gilfillan, D., Gkritzalis, T., Gregor, L., Gruber, N., Harris, I., Hartung, K., Haverd, V., Houghton, R.A., Ilyina, T., Jain, A.K., Joetzjer, E., Kadono, K., Kato, E., Kitidis, V., Korsbakken, J.I., Landschützer, P., Lefèvre, N., Lenton, A., Lienert, S., Liu, Z., Lombardozzi, D., Marland, G., Metzl, N., Munro, D.R., Nabel, J.E.M.S., Nakaoka, S.I., Niwa, Y., O'Brien, K., Ono, T., Palmer, P.I., Pierrot, D., Poulter, B., Resplandy, L., Robertson, E., Rödenbeck, C., Schwinger, J., Séférian, R., Skjelvan, I., Smith, A.J.P., Sutton, A.J., Tanhua, T., Tans, P.P., Tian, H., Tilbrook, B., Van Der Werf, G., Vuichard, N., Walker, A.P., Wanninkhof, R., Watson, A.J., Willis, D., Wiltshire, A.J., Yuan, W., Yue, X., Zaehle, S., 2020. Global Carbon Budget 2020. Earth Syst. Sci. Data 12, 3269–3340. https://doi.org/10.5194/essd-12-3269-2020

Gallagher, M.W., Nemitz, E., Dorsey, J.R., Fowler, D., Sutton, M.A., Flynn, M., Duyzer, J., 2002. Measurements and parameterizations of small aerosol deposition velocities to grassland, arable crops, and forest: Influence of surface roughness length on deposition. J. Geophys. Res. Atmos. 107, 4154. https://doi.org/10.1029/2001JD000817

Granier, C., Müller, J.-F., Brasseur, G., 2000. The Impact of Biomass Burning on the Global Budget of Ozone and

Ozone Precursors. Springer, Dordrecht, pp. 69–85. https://doi.org/10.1007/0-306-47959-1_5

Helin, A., Niemi, J. V., Virkkula, A., Pirjola, L., Teinilä, K., Backman, J., Aurela, M., Saarikoski, S., Rönkkö, T., Asmi, E., Timonen, H., 2018. Characteristics and source apportionment of black carbon in the Helsinki metropolitan area, Finland. Atmos. Environ. 190, 87–98. https://doi.org/10.1016/j.atmosenv.2018.07.022

Herich, H., Hueglin, C., Buchmann, B., 2011. A 2.5 year's source apportionment study of black carbon from wood burning and fossil fuel combustion at urban and rural sites in Switzerland. Atmos. Meas. Tech. 4, 1409–1420. https://doi.org/10.5194/amt-4-1409-2011

Hersbach, H., Bell, B., Berrisford, P., Hirahara, S., Horányi, A., Muñoz- Sabater, J., Nicolas, J., Peubey, C., Radu, R., Schepers, D., Simmons, A., Soci, C., Abdalla, S., Abellan, X., Balsamo, G., Bechtold, P., Biavati, G., Bidlot, J., Bonavita, M., Chiara, G., Dahlgren, P., Dee, D., Diamantakis, M., Dragani, R., Flemming, J., Forbes, R., Fuentes, M., Geer, A., Haimberger, L., Healy, S., Hogan, R.J., Hólm, E., Janisková, M., Keeley, S., Laloyaux, P., Lopez, P., Lupu, C., Radnoti, G., Rosnay, P., Rozum, I., Vamborg, F., Villaume, S., Thépaut, J., 2020. The ERA5 global reanalysis. Q. J. R. Meteorol. Soc. 146, 1999–2049. https://doi.org/10.1002/qj.3803

Hirsch, E., Koren, I., 2021. Record-breaking aerosol levels explained by smoke injection into the stratosphere. Science 371, 1269–1274. https://doi.org/10.1126/science.abe1415

Hodshire, A.L., Akherati, A., Alvarado, M.J., Brown-Steiner, B., Jathar, S.H., Jimenez, J.L., Kreidenweis, S.M., Lonsdale, C.R., Onasch, T.B., Ortega, A.M., Pierce, J.R., 2019. Aging Effects on Biomass Burning Aerosol Mass and Composition: A Critical Review of Field and Laboratory Studies. Environ. Sci. Technol. 53, 10007–10022. https://doi.org/10.1021/acs.est.9b02588

Hooghiem, J.J.D., Popa, M.E., Röckmann, T., Grooß, J.-U., Tritscher, I., Müller, R., Kivi, R., Chen, H., 2020. Wildfire smoke in the lower stratosphere identified by in situ CO observations. Atmos. Chem. Phys. 20, 13985–14003. https://doi.org/10.5194/acp-20-13985-2020

Jaffe, D.A., Wigder, N.L., 2012. Ozone production from wildfires: A critical review. Atmos. Environ. 51, 1–10. https://doi.org/10.1016/j.atmosenv.2011.11.063

Jiang, Z., Grosselin, B., Daële, V., Mellouki, A., Mu, Y., 2017. Seasonal and diurnal variations of BTEX compounds in the semi-urban environment of Orleans, France. Sci. Total Environ. 574, 1659–1664. https://doi.org/10.1016/j.scitotenv.2016.08.214

Jost, C., Trentmann, J., Sprung, D., Andreae, M.O., McQuaid, J.B., Barjat, H., 2003. Trace gas chemistry in a young biomass burning plume over Namibia: Observations and model simulations. J. Geophys. Res. Atmos. 108. https://doi.org/10.1029/2002JD002431

Kalogridis, A.C., Vratolis, S., Liakakou, E., Gerasopoulos, E., Mihalopoulos, N., Eleftheriadis, K., 2018. Assessment of wood burning versus fossil fuel contribution to wintertime black carbon and carbon monoxide concentrations in Athens, Greece. Atmos. Chem. Phys. 18, 10219–10236. https://doi.org/10.5194/acp-18-10219-2018

Kloss, C., Berthet, G., Sellitto, P., Ploeger, F., Bucci, S., Khaykin, S., Jégou, F., Taha, G., Thomason, L.W., Barret, B., Le Flochmoen, E., Von Hobe, M., Bossolasco, A., Bègue, N., Legras, B., 2019. Transport of the 2017 canadian wildfire plume to the tropics via the asian monsoon circulation. Atmos. Chem. Phys. 19, 13547–

13567. https://doi.org/10.5194/acp-19-13547-2019

Kloss, C., Sellitto, P., von Hobe, M., Berthet, G., Smale, D., Krysztofiak, G., Xue, C., Qiu, C., Jégou, F., Ouerghemmi, I., Legras, B., 2021. Australian Fires 2019–2020: Tropospheric and Stratospheric Pollution Throughout the Whole Fire Season. Front. Environ. Sci. 9, 1–11. https://doi.org/10.3389/fenvs.2021.652024

Krysztofiak, G., Catoire, V., Hamer, P.D., Marécal, V., Robert, C., Engel, A., Bönisch, H., Grossmann, K., Quack, B., Atlas, E., Pfeilsticker, K., 2018. Evidence of convective transport in tropical West Pacific region during SHIVA experiment. Atmos. Sci. Lett. 19, 1–7. https://doi.org/10.1002/asl.798

Li, S., Liu, D., Hu, D., Kong, S., Wu, Y., Ding, S., Cheng, Y., Qiu, H., Zheng, S., Yan, Q., Zheng, H., Hu, K., Zhang, J., Zhao, D., Liu, Q., Sheng, J., Ye, J., He, H., Ding, D., 2021. Evolution of Organic Aerosol From Wood Smoke Influenced by Burning Phase and Solar Radiation. J. Geophys. Res. Atmos. 126, 1–16. https://doi.org/10.1029/2021JD034534

Liu, Y., Stanturf, J., Goodrick, S., 2010. Trends in global wildfire potential in a changing climate. For. Ecol. Manage. 259, 685–697. https://doi.org/10.1016/j.foreco.2009.09.002

Mellouki, A., Ammann, M., Cox, R.A., Crowley, J.N., Herrmann, H., Jenkin, M.E., McNeill, V.F., Troe, J., Wallington, T.J., 2021. Evaluated kinetic and photochemical data for atmospheric chemistry: volume VIII – gas-phase reactions of organic species with four, or more, carbon atoms (≥ C₄). Atmos. Chem. Phys. 21, 4797–4808. https://doi.org/10.5194/acp-21-4797-2021

Nie, W., Ding, A.J., Xie, Y.N., Xu, Z., Mao, H., Kerminen, V.-M., Zheng, L.F., Qi, X.M., Huang, X., Yang, X.-Q., Sun, J.N., Herrmann, E., Petäjä, T., Kulmala, M., Fu, C.B., 2015. Influence of biomass burning plumes on HONO chemistry in eastern China. Atmos. Chem. Phys. 15, 1147–1159. https://doi.org/10.5194/acp-15-1147-2015

Peng, Q., Palm, B.B., Melander, K.E., Lee, B.H., Hall, S.R., Ullmann, K., Campos, T., Weinheimer, A.J., Apel, E.C., Hornbrook, R.S., Hills, A.J., Montzka, D.D., Flocke, F., Hu, L., Permar, W., Wielgasz, C., Lindaas, J., Pollack, I.B., Fischer, E. V., Bertram, T.H., Thornton, J.A., 2020. HONO Emissions from Western U.S. Wildfires Provide Dominant Radical Source in Fresh Wildfire Smoke. Environ. Sci. Technol. 54, 5954–5963. https://doi.org/10.1021/acs.est.0c00126

Pisso, I., Sollum, E., Grythe, H., Kristiansen, N.I., Cassiani, M., Eckhardt, S., Arnold, D., Morton, D., Thompson, R.L., Groot Zwaaftink, C.D., Evangeliou, N., Sodemann, H., Haimberger, L., Henne, S., Brunner, D., Burkhart, J.F., Fouilloux, A., Brioude, J., Philipp, A., Seibert, P., Stohl, A., 2019. The Lagrangian particle dispersion model FLEXPART version 10.4. Geosci. Model Dev. 12, 4955–4997. https://doi.org/10.5194/gmd-12-4955-2019

Quegan, S., Le Toan, T., Chave, J., Dall, J., Exbrayat, J.F., Minh, D.H.T., Lomas, M., D'Alessandro, M.M., Paillou, P., Papathanassiou, K., Rocca, F., Saatchi, S., Scipal, K., Shugart, H., Smallman, T.L., Soja, M.J., Tebaldini, S., Ulander, L., Villard, L., Williams, M., 2019. The European Space Agency BIOMASS mission: Measuring forest above-ground biomass from space. Remote Sens. Environ. https://doi.org/10.1016/j.rse.2019.03.032

R'Honi, Y., Clarisse, L., Clerbaux, C., Hurtmans, D., Duflot, V., Turquety, S., Ngadi, Y., Coheur, P.F., 2013.

Exceptional emissions of NH_3 and HCOOH in the 2010 Russian wildfires. Atmos. Chem. Phys. 13, 4171–4181. https://doi.org/10.5194/acp-13-4171-2013

Ramo, R., Roteta, E., Bistinas, I., van Wees, D., Bastarrika, A., Chuvieco, E., van der Werf, G.R., 2021. African burned area and fire carbon emissions are strongly impacted by small fires undetected by coarse resolution satellite data. Proc. Natl. Acad. Sci. 118, e2011160118. https://doi.org/10.1073/pnas.2011160118

Randerson, J.T., Chen, Y., van der Werf, G.R., Rogers, B.M., Morton, D.C., 2012. Global burned area and biomass burning emissions from small fires. J. Geophys. Res. Biogeosciences 117, G4012. https://doi.org/10.1029/2012JG002128

Saunois, M., Stavert, A.R., Poulter, B., Bousquet, P., Canadell, J.G., Jackson, R.B., Raymond, P.A., Dlugokencky, E.J., Houweling, S., Patra, P.K., Ciais, P., Arora, V.K., Bastviken, D., Bergamaschi, P., Blake, D.R., Brailsford, G., Bruhwiler, L., Carlson, K.M., Carrol, M., Castaldi, S., Chandra, N., Crevoisier, C., Crill, P.M., Covey, K., Curry, C.L., Etiope, G., Frankenberg, C., Gedney, N., Hegglin, M.I., Höglund-Isaksson, L., Hugelius, G., Ishizawa, M., Ito, A., Janssens-Maenhout, G., Jensen, K.M., Joos, F., Kleinen, T., Krummel, P.B., Langenfelds, R.L., Laruelle, G.G., Liu, L., Machida, T., Maksyutov, S., McDonald, K.C., McNorton, J., Miller, P.A., Melton, J.R., Morino, I., Müller, J., Murguia-Flores, F., Naik, V., Niwa, Y., Noce, S., O'Doherty, S., Parker, R.J., Peng, C., Peng, S., Peters, G.P., Prigent, C., Prinn, R., Ramonet, M., Regnier, P., Riley, W.J., Rosentreter, J.A., Segers, A., Simpson, I.J., Shi, H., Smith, S.J., Steele, L.P., Thornton, B.F., Tian, H., Tohjima, Y., Tubiello, F.N., Tsuruta, A., Viovy, N., Voulgarakis, A., Weber, T.S., van Weele, M., van der Werf, G.R., Weiss, R.F., Worthy, D., Wunch, D., Yin, Y., Yoshida, Y., Zhang, W., Zhang, Z., Zhao, Y., Zheng, B., Zhu, Qing, Zhu, Qiuan, Zhuang, Q., 2020. The Global Methane Budget 2000–2017. Earth Syst. Sci. Data 12, 1561–1623. https://doi.org/10.5194/essd-12-1561-2020

Seiler, W., Crutzen, P.J., 1980. Estimates of gross and net fluxes of carbon between the biosphere and the atmosphere from biomass burning. Clim. Change. https://doi.org/10.1007/BF00137988

Seinfeld, J.H., Pandis, S.N., 2016. Atmospheric Chemistry and Physics: From Air Pollution to Climate Change, John Wiley & Sons. John Wiley & Sons.

Tang, Y.S., Flechard, C.R., Dämmgen, U., Vidic, S., Djuricic, V., Mitosinkova, M., Uggerud, H.T., Sanz, M.J., Simmons, I., Dragosits, U., Nemitz, E., Twigg, M., van Dijk, N., Fauvel, Y., Sanz, F., Ferm, M., Perrino, C., Catrambone, M., Leaver, D., Braban, C.F., Cape, J.N., Heal, M.R., Sutton, M.A., 2021. Pan-European rural monitoring network shows dominance of NH_3 gas and NH_4NO_3 aerosol in inorganic atmospheric pollution load. Atmos. Chem. Phys. 21, 875–914. https://doi.org/10.5194/acp-21-875-2021

Theys, N., Volkamer, R., Müller, J.-F., Zarzana, K.J., Kille, N., Clarisse, L., De Smedt, I., Lerot, C., Finkenzeller, H., Hendrick, F., Koenig, T.K., Lee, C.F., Knote, C., Yu, H., Van Roozendael, M., 2020. Global nitrous acid emissions and levels of regional oxidants enhanced by wildfires. Nat. Geosci. 13, 681–686. https://doi.org/10.1038/s41561-020-0637-7

Van Der Werf, G.R., Randerson, J.T., Giglio, L., Van Leeuwen, T.T., Chen, Y., Rogers, B.M., Mu, M., Van Marle, M.J.E., Morton, D.C., Collatz, G.J., Yokelson, R.J., Kasibhatla, P.S., 2017. Global fire emissions estimates during 1997-2016. Earth Syst. Sci. Data 9, 697–720. https://doi.org/10.5194/essd-9-697-2017

Wang, S., Coggon, M.M., Gkatzelis, G.I., Warneke, C., Bourgeois, I., Ryerson, T., Peischl, J., Veres, P.R., Neuman, J.A., Hair, J., Shingler, T., Fenn, M., Diskin, G., Huey, L.G., Lee, Y.R., Apel, E.C., Hornbrook, R.S., Hills, A.J., Hall, S.R., Ullmann, K., Bela, M.M., Trainer, M.K., Kumar, R., Orlando, J.J., Flocke, F.M., Emmons, L.K., 2021. Chemical Tomography in a Fresh Wildland Fire Plume: A Large Eddy Simulation (LES) Study. J. Geophys. Res. Atmos. 126. https://doi.org/10.1029/2021JD035203

Wiedinmyer, C., Akagi, S.K., Yokelson, R.J., Emmons, L.K., Al-Saadi, J.A., Orlando, J.J., Soja, A.J., 2011. The Fire INventory from NCAR (FINN): A high resolution global model to estimate the emissions from open burning. Geosci. Model Dev. 4, 625–641. https://doi.org/10.5194/gmd-4-625-2011

Xu, L., Crounse, J.D., Vasquez, K.T., Allen, H., Wennberg, P.O., Bourgeois, I., Brown, S.S., Campuzano-Jost, P., Coggon, M.M., Crawford, J.H., DiGangi, J.P., Diskin, G.S., Fried, A., Gargulinski, E.M., Gilman, J.B., Gkatzelis, G.I., Guo, H., Hair, J.W., Hall, S.R., Halliday, H.A., Hanisco, T.F., Hannun, R.A., Holmes, C.D., Huey, L.G., Jimenez, J.L., Lamplugh, A., Lee, Y.R., Liao, J., Lindaas, J., Neuman, J.A., Nowak, J.B., Peischl, J., Peterson, D.A., Piel, F., Richter, D., Rickly, P.S., Robinson, M.A., Rollins, A.W., Ryerson, T.B., Sekimoto, K., Selimovic, V., Shingler, T., Soja, A.J., St. Clair, J.M., Tanner, D.J., Ullmann, K., Veres, P.R., Walega, J., Warneke, C., Washenfelder, R.A., Weibring, P., Wisthaler, A., Wolfe, G.M., Womack, C.C., Yokelson, R.J., 2021. Ozone chemistry in western U.S. wildfire plumes. Sci. Adv. 7. https://doi.org/10.1126/sciadv.abl3648

Yttri, K.E., Lund Myhre, C., Eckhardt, S., Fiebig, M., Dye, C., Hirdman, D., Ström, J., Klimont, Z., Stohl, A., 2014. Quantifying black carbon from biomass burning by means of levoglucosan - A one-year time series at the Arctic observatory Zeppelin. Atmos. Chem. Phys. 14, 6427–6442. https://doi.org/10.5194/acp-14-6427-2014

Yu, P., Toon, O.B., Bardeen, C.G., Zhu, Y., Rosenlof, K.H., Portmann, R.W., Thornberry, T.D., Gao, R.-S., Davis, S.M., Wolf, E.T., de Gouw, J., Peterson, D.A., Fromm, M.D., Robock, A., 2019. Black carbon lofts wildfire smoke high into the stratosphere to form a persistent plume. Science 365, 587–590. https://doi.org/10.1126/science.aax1748

Zheng, B., Chevallier, F., Yin, Y., Ciais, P., Fortems-Cheiney, A., Deeter, M.N., Parker, R.J., Wang, Y., Worden, H.M., Zhao, Y., 2019. Global atmospheric carbon monoxide budget 2000–2017 inferred from multi-species atmospheric inversions. Earth Syst. Sci. Data 11, 1411–1436. https://doi.org/10.5194/essd-11-1411-2019